10th World Congress on Structural and Multidisciplinary Optimization
May 19 - 24, 2013, Orlando, Florida, USA

Aircraft Loft Optimization With Respect to Aeroelastic Lift and Induced Drag Loads

S. Deinert*, Ö. Petersson†, F. Daoud‡, H. Baier§

*Cassidian, Manching, Germany, sebastian.deinert@cassidian.com
†Cassidian, Manching, Germany, oegmundur.petersson@cassidian.com
‡Cassidian, Manching, Germany, fernass.daoud@cassidian.com
§Technical University of Munich, Garching, Germany, baier@llb.mw.tum.de

1. Abstract
The search for a good aircraft configuration during the conceptual design phase has great influence on the overall aircraft performance and requires consideration of many different aspects with strong interrelations. This paper describes a multidisciplinary shape optimization framework for application as early as this design phase. It allows fully coupled aeroelastic shape optimization of aircraft and consists of three components, a parametric geometry kernel, a multidisciplinary design optimization program and an aerodynamic solver. For parametric geometry description, the CPACS data format [7] developed by DLR is utilized. Aerodynamic influence coefficient matrices are employed to enable time efficient aeroelastic analysis. Especially induced drag evaluation is regarded during aeroelastic analysis, due to its high sensitivity to elastic deformations. The capabilities of the framework are demonstrated using two optimization examples and the influence of coupled problems on the overall optimum is shown.

2. Keywords
Optimization, Shape, Aeroelasticity, Induced Drag

3. Multidisciplinary Shape Optimization in Conceptual Aircraft Design
During an aircraft's conceptual design phase, the main task is to find the best feasible aircraft concept for a given design mission. Therefore, it is the engineer's responsibility to select the one aircraft configuration out of usually several different concepts with the highest performance satisfying all requirements. Since all subsequent design phases will use this design for further development, this decision has a strong influence on the performance of the final aircraft. To provide a good foundation for the selection, numerical analysis tools combined with statistical methods help the conceptual engineer to estimate the performance of a design concept with respect to a specific requirement. However, due to the great number of the different aspects that must be considered, it is very difficult to cover the whole design space manually with numerical analyses in an efficient manner.
For this application, a multidisciplinary shape optimization framework is being developed at Cassidian. One major advantage of multidisciplinary design optimization (MDO) in this context is that it allows finding an optimized configuration, which satisfies all considered design constraints. Thus, MDO helps exploring a given design space effectively. Sequential treatment of these criteria usually holds difficulties when trying to find a solution that satisfies all of them caused by their interdependencies. Aeroelasticity is one example for this; structural elastification affects the flow around a body (e.g. a wing) which causes lift and drag forces that influence the elastic deformation of the body itself. Therefore, this problem has to be solved in a coupled manner. Multidisciplinary design optimization is very well suited for finding concepts with good properties regarding such coupled problems, however, one has to keep in mind that any constraint not included during the optimization usually is found violated when evaluating the resulting optimized design. Therefore, in order to find "globally feasible" designs that serve as valid starting points for all disciplines in the following design phases, a comprehensive design criteria model must be provided. Over the time line of the aircraft development process, design criteria may change frequently with the development phases up to the final set of constraints required for certification. By using MDO design criteria that are as close as possible to those final certification constraints already early on in the development process, one can minimize the occurrence of design reiteration loops caused by new or significantly changed design criteria.
The usage of shape optimization offers far greater design freedom than for example the traditional sizing optimization, which only alters the dimensions of structural components but keeps the shape of the design

constant. As opposed to topology optimization, which distributes material in a fixed design volume in order to improve the objective, shape optimization uses a given topology and modifies its shape in order to reach the optimum. Therefore, the parameters used to influence the design are almost conventional engineering parameters, which facilitates manufacturing and also the definition of form constraints. Shape changes are usually applied to existing analysis meshes (e.g. structural finite element or aerodynamic finite volume mesh) by moving mesh nodes or deforming an overlying geometric representation to which the analyses meshes are linked. Originating from these mesh deformations, numerical issues may arise in the analysis methods leading to incorrect results that might compromise the optimization. Also, if gradient based optimization algorithms are employed for shape optimization, the derivatives of objective and constraint functions with respect to the deformation of analysis meshes have to be calculated. Especially for multidisciplinary optimization with several different analysis models, shape optimization adds substantial complexity compared to multidisciplinary sizing optimization.
The developed framework offers the features of multidisciplinary design optimization to aircraft development phases as early as the conceptual stage with the added design freedom provided by shape optimization. Yet, through a modular architecture the framework will offer multi-fidelity application for the future. This means that the employed analysis methods can increase in complexity and accuracy (e.g. exchanging potential theory aerodynamics with Navier-Stokes) throughout the different development phases as the aircraft design matures.

4. Shape MDO Framework

Three main components establish the shape optimization framework. These are the in-house MDO program *LAGRANGE* [9], the parametric geometry program *DescartesNDB* (Descartes Numerical Design Board), also developed in-house, as well as an aerodynamic solver (e.g. *AVL* (*Athena Vortex Lattice* [2])). Linking these programs together via a common database and design variable model allows multidisciplinary shape optimization with aeroelastic analysis and updated loads.

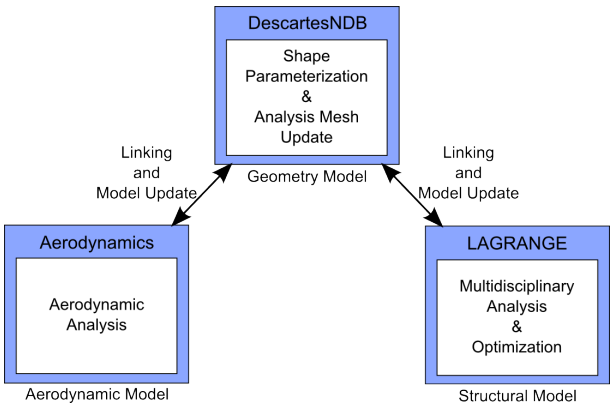

Figure 1: Overview of the shape MDO framework

Figure 1 shows how the different analysis models are linked to the central parametric geometry model in *DescartesNDB*. Additionally, this figure illustrates the tasks handled by each of the components in the framework. These functions will be described more in detail in the following sections.

4.1 Shape Parametrization with *DescartesNDB*

DescartesNDB (see Figure 2) is an enhanced version of the open source program *TIGLViewer* developed by the DLR (German Aerospace Center) [7]. Both programs are based on the parametric aircraft description format CPACS (Common Parametric Aircraft Configuration Schema), which is also developed by the DLR [7]. The CPACS data format allows definition of a complete aircraft via XML code including geometric, structural, performance and meta data among others. The parameters used to describe the aircraft in this format consist of everyday aerospace engineering terms (e.g. chord length, sweep angle, etc.). With the wide set of shape parameters available in CPACS a great variety of geometry changes can be realized ranging from large modifications, such as position of the main wing, up to very local deformations like the position of a point in the aerodynamic profile of an airfoil. Another big advantage of the CPACS format for shape optimization is the inherent consistency of parameters reducing the probability of creating impossible geometry configurations. Enhancements made to the *TIGLViewer*, which

was intended as a viewing tool for CPACS datasets using the *Open Cascade* geometric kernel [8], added the ability of generating and managing analysis meshes as well as defining shape design variables.

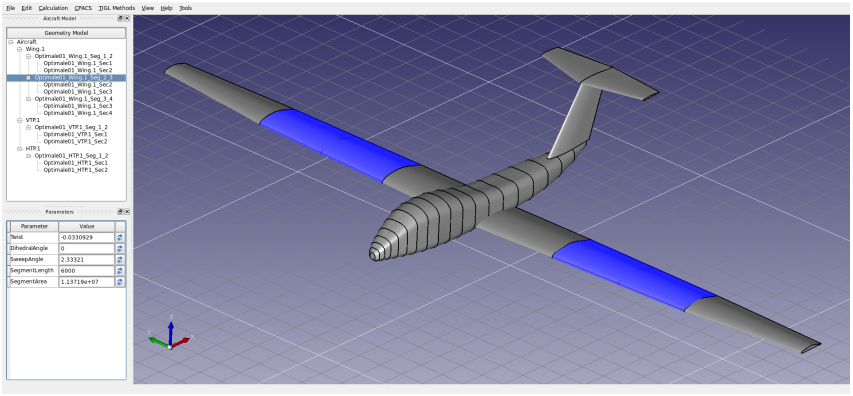

Figure 2: Screenshot of the *DescartesNDB* GUI

For shape parametrization, all necessary analysis models are generated from a given CPACS dataset. This can happen externally or in *DescartesNDB* itself. The created models are then linked to the geometric CPACS model. This linking generally involves mapping mesh nodes onto the geometric surfaces of the CPACS model through relative coordinates. *DescartesNDB* applies this information to update the analysis meshes once a shape parameter is changed. Due to the connection to the higher logic of the geometry model, even large shape changes can be managed without deteriorating the quality of the linked analysis meshes to the point, where re-meshing is required to prevent numerical problems in the analysis solvers. Also, through this approach, the mesh topologies remain unchanged throughout a shape optimization, which minimizes data managing effort when providing the meshes to their analysis programs.
Definition of shape design variables is also done in *DescartesNDB* based on the parametric geometry model. Any CPACS parameter or some additionally included higher parameters (e.g. overall wing span) may be set as shape design variables. Lower and upper gages have to be specified for each shape design variable before all variable data is written to file and handed over to the optimization program.
With analysis model linking and shape design variables defined, *DescartesNDB* is then able to alter the shape of the geometry and the linked models uniformly once a shape design variable value is changed. This guarantees consistency between the involved disciplines. Where necessary, *DescartesNDB* can also initiate re-analyses of certain analysis models.

4.2 Multidisciplinary Analysis/Optimization with *LAGRANGE*

The second component of the presented framework is the in-house multidisciplinary design optimization program *LAGRANGE* [9]. It has been developed over the last 30 years at Cassidian and features its own structural finite element solver. An extensive design criteria model has been added during this development, which includes for example strength, stability, manufacturing, aeroelastic effectiveness, trimming, flutter, gust as well as modal constraints. Different gradient based optimization algorithms are included in *LAGRANGE* for selection according to the optimization problem at hand. Gradients necessary for the optimizer are calculated fully analytically. Due to this, *LAGRANGE* can conduct sizing or layer angle optimizations with large numbers of design variables (more than 10^4) combined with a substantial design criteria model (over 10^7 constraints).
One of the most important analysis types for aircraft development is the coupled aeroelastic analysis. For this, *LAGRANGE* can be combined with different potential theory aerodynamic codes (e.g. *AVL*, *DLM* [1] or *HISSS* [3]). These aerodynamic codes calculate so called aerodynamic influence coefficient (AIC) matrices (see [4], [1]) in preparation of aeroelastic analysis. AIC matrices provide a linear relationship between the boundary condition vector and the singularity strength ultimately leading to the pressure distribution. This yields a good linear approximation to the solution of the flow conditions. Since the aeroelastic problem is solved iteratively, the use of AIC matrices saves a significant amount of computation time compared to repeatedly calling an aerodynamic solver.
The basic equation for the structural finite element problem is given in Eq.(1):

$$\mathbf{K} \cdot \mathbf{u} = \mathbf{F}_{St} \tag{1}$$

In Eq.(1) the product of stiffness matrix $\mathbf{K}$ with the displacement vector $\mathbf{u}$ equals the static force vector $\mathbf{F}_{St}$. The aeroelastic analysis considers aerodynamic forces $\mathbf{F}_{Ae}$ originating from an aerodynamic pressure distribution that is dependent on the structural displacements. Adding these forces to the static equation leads to the aeroelastic relation of Eq.(2):

$$\begin{aligned} \mathbf{K} \cdot \mathbf{u} &= \mathbf{F}_{St} + \mathbf{F}_{Ae} \\ \mathbf{F}_{Ae} &= \mathbf{F}_{Ae_0} + \mathbf{C} \cdot \mathbf{u} \\ \mathbf{C} &= q \cdot \mathbf{S}^T \cdot \mathbf{P} \cdot \mathbf{A}_{C_P} \cdot \mathbf{S} \end{aligned} \tag{2}$$

Thus, the static equation turns into an implicit equation due to this dependency on the displacement vector $\mathbf{u}$ of both sides represented by $\mathbf{K}$ and $\mathbf{C}$ (Eq.(2)). In this case, $\mathbf{C}$ is defined for an AIC matrix originating from an aerodynamic vortex lattice method (i.e. *AVL*). It is calculated using the coupling matrix $\mathbf{S}$, the aerodynamic panel area matrix $\mathbf{P}$, the dynamic pressure q and the AIC matrix $\mathbf{A}_{C_P}$ itself. Eq.(2) is solved iteratively in *LAGRANGE* for the displacement $\mathbf{u}$ starting with the initial rigid aerodynamic load $\mathbf{F}_{Ae_0}$. The structural displacements mainly affect the aerodynamic solution through changes in the boundary condition much more than through deformation of the aerodynamic model. Hence, the AIC matrix provides a good approximation for the aerodynamic solution. Therefore, $\mathbf{u}$ is used to calculate the new aerodynamic boundary condition in order to determine the current aerodynamic load vector $\mathbf{F_{Ae}}$ for each pass in the aeroelastic iteration loop. However, in case of shape optimization, where the shape design variables cause much greater form changes, the AIC matrices have to be recalculated with every shape update. This increases computational time, yet, the aerodynamic solver has to be called only once per optimization iteration, while the function evaluations still profit from the usage of AIC matrices.

The open source vortex lattice code *AVL* was extended for this work to create AIC matrices that enable an induced drag Trefftz Plane analysis [10] in *LAGRANGE*. For this feature, an induced drag AIC matrix, additional to the one used in the equations above, is introduced. Via this matrix it is possible to determine the aerodynamic lift distribution as well as the induced drag coefficient for coupled aeroelastic flight states. The aeroelastic induced drag calculated with this method can be defined as an objective function during an optimization. The generation of the induced drag AIC mentioned here will be discussed more in detail in section 4.3.

LAGRANGE is included into the framework joining its features with the parametric geometry description of CPACS and *DescartesNDB* for multidisciplinary shape optimization. This way, shape design variables defined in *DescartesNDB* can be combined with the sizing or composite layer angle design variables from *LAGRANGE*. Hence, for example, a coupled sizing and shape optimization can be conducted to find a good aircraft concept. With this approach, *LAGRANGE* can use shape design variables that influence multiple analysis disciplines with the full extent of its existing program logic, while *DescartesNDB* handles the complexity of the relations between different analysis models and their shape modifications.

4.3 Aerodynamic Analysis with *AVL*

The third component of the developed shape MDO framework is the aerodynamic solver. This is an optional module in the framework required for aeroelastic optimization. In general, the framework is designed in such way that this component can be exchanged easily to allow different fidelity levels of aerodynamic solvers. For application of the shape MDO framework in the conceptual aircraft design stage, the vortex lattice solver Athena Vortex Lattice (*AVL*), developed at the Massachusetts Institute of Technology [2], is chosen. Yet, higher order methods such as panel, Euler or Navier-Stokes solvers may also be included in the future.

AVL (Figure 3) is very well adapted to the needs of conceptual design. A model is constructed from the plan form of an aircraft using measurements such as span, chord length, airfoil profiles and sweep/dihedral angles; parameters that are readily available at this stage. With this information, *AVL* describes aerodynamic bodies through 2D plates that may feature camber or twist. This allows fast computation times with a suitable accuracy of results. The previously mentioned ability to calculate induced drag represents a useful feature in the search for good aircraft concepts, since a large fraction of the overall drag force during flight is constituted by induced drag. This drag component is of special interest during conceptual design, because it can be influenced effectively by parameters that are determined during this phase

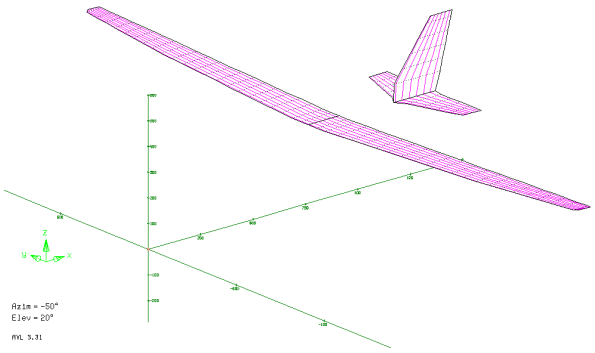

Figure 3: Example for an Athena Vortex Lattice model

(e.g. wing span, aspect ratio etc.). It also shows a strong sensitivity to changes in lift distribution caused by the aeroelastic effects mentioned earlier. One major limitation of this aerodynamic method is the reliability of results when calculating flow conditions in the transonic Mach region ($0.8 < Ma < 1.2$). Here, compressibility effects and other non-linearities have great influence on the flow, which cannot be described accurately enough with potential theory methods (such as *AVL*). Therefore, higher fidelity methods should be used in transonic regions. Since this current application focuses on long endurance unmanned aerial vehicles (UAV), which are designed rather for efficient sail plane characteristics, these problems will not impede the usage of *AVL*.
In order to couple *AVL* with *LAGRANGE*, certain features have been added to the program so that it enables output of the, before mentioned, aerodynamic influence coefficient matrices (see e.g. [1]).

$$\mathbf{A} \cdot \mathbf{\Gamma} = \mathbf{b_N} \tag{3}$$

Eq.(3) describes the basic equation system of a vortex lattice method such as *AVL*. The product of the aerodynamic influence matrix $\mathbf{A}$ with the singularity strength vector $\mathbf{\Gamma}$ of each panel equals the Neumann boundary conditions $\mathbf{b_N}$ over all panels. During analysis, Eq.(3) is solved for $\mathbf{\Gamma}$ and these values can be converted to pressure difference coefficient values for each panel i in a post-processing step as shown in Eq.(4).

$$\Delta C_{Pi} = \frac{2}{P_i} \Gamma_i \cdot \mathbf{n}_i \cdot (\mathbf{v}_i \times \mathbf{l}_i) \tag{4}$$

Using the singularity strength Γ_i together with the panel area P_i, the panel normal vector $\mathbf{n}_i$, the flow velocity vector $\mathbf{v}_i$ and the length of the vortex element $\mathbf{l}_i$ in the panel yields the pressure difference coefficient for panel i. This ΔC_{Pi} is then applied for evaluation of aerodynamic loads during aeroelastic analysis. However, in order to obtain an AIC matrix as described in section 4.2, one has to combine the solution of Eq.(3) and the post processing step of Eq.(4) into a single matrix. After some conversions the pressure difference AIC matrix is defined as:

$$\mathbf{A}_{C_P} = -\frac{2}{c_i} \cdot A_{ij}^{-1} \tag{5}$$

Eq.(5) relates the pressure coefficient matrix introduced in Eq.(2) with the inverted aerodynamic influence matrix from Eq.(3) using the mean chord length c_i of each panel i. Handing this matrix over to *LAGRANGE*, enables the fully coupled aeroelastic analysis that was described earlier. The pressure coefficient AIC matrix only depends on the geometry of the aerodynamic panel model as well as the Mach number (through Prandtl-Glauert transformation). Therefore, the same matrix can be used for any possible flight state with the corresponding Mach number as long as the shape of the aerodynamic model remains unchanged.
The induced drag AIC matrix, also mentioned in section 4.2, relies on the solution of Eq.(3) as well. Here, the singularity strength vector $\mathbf{\Gamma}$ is fed into the Trefftz Plane analysis [10] to calculate the induced drag coefficient. During Trefftz Plane analysis, downwash velocities are evaluated in a plane that is located infinitely far behind the aircraft, perpendicular to the direction of motion. Integration over these velocities in the Trefftz Plane allows an estimation of the induced drag value.

$$D_{ind} = -\frac{\rho}{2} \sum_{i=1}^{n_P} \Gamma_i w_{ind_i} b_i \tag{6}$$

Eq.(6) shows that relation of downwash velocity w_{ind} and the induced drag force D_{ind} for a discretized vortex lattice formulation (see for example [5]). Summation over all panels n_P of the product of singularity strength Γ_i, downwash velocity w_{ind_i} and panel span b_i for panel i produces the overall induced drag force. The downwash velocity itself is dependent on the singularity strength vector as well:

$$\mathbf{w_{ind}} = \mathbf{A_w} \cdot \mathbf{\Gamma} \tag{7}$$

In Eq.(7), $\mathbf{A_w}$ denotes the downwash influence matrix which is similar to $\mathbf{A}$ in Eq.(3), however, set up in the Trefftz Plane. After a number of conversions one can find the dependency shown in Eq.(8) (a similar approach was shown in [6]):

$$C_{D_{ind}} = \mathbf{\Gamma}^T \mathbf{A_D} \mathbf{\Gamma} \tag{8}$$

The induced drag AIC matrix $\mathbf{A_D}$ can be handed over to an external program like *LAGRANGE* to be applied for calculation of the elastic overall induced drag coefficient $C_{D_{ind}}$. Additionally, required to obtain $\mathbf{\Gamma}$, the inverted aerodynamic influence matrix $\mathbf{A^{-1}}$ from Eq.(3) is also transferred to *LAGRANGE*. During aeroelastic analysis, the Neumann boundary conditions are calculated from the displacement vector, multiplied with the inverted aerodynamic influence matrix and then inserted into Eq.(8) for induced drag coefficient evaluation. The two influence matrices $\mathbf{A_D}$ and $\mathbf{A^{-1}}$ have the same characteristics as the pressure coefficient AIC matrix $\mathbf{A}_{C_P}$ and, therefore, only need to be updated once a shape change to the aerodynamic model occurred.
Thus, *AVL* is called in the shape MDO framework by *DescartesNDB* every time a shape update affects the aerodynamic model. It then re-calculates the three aerodynamic influence coefficient matrices and stores them on file, which is subsequently read by *LAGRANGE* for aeroelastic analysis.

4.4 Sensitivity Analysis

An optimization applying gradient based optimizers requires calculation of sensitivities for the objective function f as well as all constraint functions g_i with respect to every defined design variable x_j. In the general case, the objective function and constraint functions depend on the design variable vector $\mathbf{x}$ but also on the displacement vector $\mathbf{u}$, which is itself dependent on $\mathbf{x}$ (Eq.(9)).

$$\begin{aligned} f &= f(\mathbf{x}, \mathbf{u}(\mathbf{x})) \\ \mathbf{g} &= \mathbf{g}(\mathbf{x}, \mathbf{u}(\mathbf{x})) \end{aligned} \tag{9}$$

In the following, several approaches for sensitivity calculation are presented for the shape MDO framework, all with respect to shape design variables. To simplify notation, this is done for one constraint function g and one design variable x only, but can be extended to more constraints and design variables without limitation.
The first method is the numerical gradient calculation using, in this case, so called forward differencing. Eq.(10) shows the gradients for objective and constraint function, computed through a difference quotient of two analysis results. Forward differencing does not require any knowledge of the involved mathematics necessary for calculating f or g. Yet, a complete analysis must be done once for each design variable plus an initial unperturbed analysis raising computational effort as the number of design variables increases.

$$\begin{aligned} \frac{df}{dx} &= \frac{f(x + \Delta x) - f(x)}{\Delta x} \\ \frac{dg}{dx} &= \frac{g(x + \Delta x) - g(x)}{\Delta x} \end{aligned} \tag{10}$$

The second approach, which is usually much more efficient with respect to computational effort, is analytical gradient calculation. This means, derivation of all involved mathematical relations is required. The great advantage of this is that a gradient evaluation only requires one analysis and one additional for gradient calculation call. The achievable accuracy is independent of the currently solved problem and is therefore more reliable than the first described method. Eq.(11) shows the analytical derivatives of f

and g split into the explicit partial derivative (direct dependency on x) and the implicit part (indirect dependency on x via displacements $\mathbf{u}$).

$$\begin{aligned} \frac{df}{dx} &= \frac{\partial f}{\partial x} + \frac{\partial f}{\partial \mathbf{u}} \cdot \frac{d\mathbf{u}}{dx} \\ \frac{dg}{dx} &= \frac{\partial g}{\partial x} + \frac{\partial g}{\partial \mathbf{u}} \cdot \frac{d\mathbf{u}}{dx} \end{aligned} \tag{11}$$

Assuming the explicit derivatives can be calculated directly, the implicit derivative usually states more of a challenge. Therefore, Eq.(12) and Eq.(13) show the derivation of the basic finite element formulation Eq.(1) and its expansion for aeroelasticity Eq.(2) with respect to a shape design variable.

$$\mathbf{K} \cdot \frac{d\mathbf{u}}{dx} = -\frac{d\mathbf{K}}{dx} \cdot \mathbf{u} + \frac{d\mathbf{F}_{St}}{dx} \tag{12}$$

$$\mathbf{K} \cdot \frac{d\mathbf{u}}{dx} = -\frac{d\mathbf{K}}{dx} \cdot \mathbf{u} + \frac{d\mathbf{F}_{St}}{dx} + \frac{d\mathbf{F}_{Ae}}{dx} \tag{13}$$

with

$$\frac{d\mathbf{F}_{Ae}}{dx} = \frac{d\mathbf{F}_{Ae_0}}{dx} + q \cdot \mathbf{S}^{\mathbf{T}} \cdot \mathbf{P} \cdot \mathbf{A}_{C_P} \cdot \mathbf{S} \cdot \frac{d\mathbf{u}}{dx} + q \cdot \mathbf{S}^{\mathbf{T}} \cdot \frac{d\mathbf{P}}{dx} \cdot \mathbf{A}_{C_P} \cdot \mathbf{S} \cdot \mathbf{u} + q \cdot \mathbf{S}^{\mathbf{T}} \cdot \mathbf{P} \cdot \frac{d\mathbf{A}_{C_P}}{dx} \cdot \mathbf{S} \cdot \mathbf{u} \tag{14}$$

Eq.(13) shows a similar dependency on the displacement as its corresponding analysis Eq.(2) and is, therefore, also solved iteratively for $\frac{d\mathbf{u}}{dx}$. The transformation $\mathbf{S}$ between aerodynamic and structural system in Eq.(14) is assumed independent of the shape variable, but might also require derivation depending on the coupling method. Multidisciplinary shape optimization requires sensitivities for mesh deformations of all involved analysis meshes, represented here by the stiffness matrix derivative $\frac{d\mathbf{K}}{dx}$ in Eq.(13), the AIC matrix derivative $\frac{d\mathbf{A}_{C_P}}{dx}$ and the panel area derivative $\frac{d\mathbf{P}}{dx}$ in Eq.(14). This demands passing derivatives between all programs in the framework as well as computation of analytical derivatives in the aerodynamic solver. For these reasons, the fully analytical gradient calculation approach is not implemented in the framework, for now.

The third method for gradient calculation described here is the semi-analytical derivation, which represents a combination of the two previously presented approaches. This means that some parts of the analytical derivation chain are calculated numerically and set into the main equation to solve analytically. The semi-analytical approach generally has the advantage of exploiting the "black-box" behaviour of numerical gradient calculation, while keeping accuracy high through analytical solution of the overall equation. In this case, equations Eq.(13) and Eq.(14) can be rewritten as:

$$\mathbf{K} \cdot \frac{d\mathbf{u}}{dx} = -\frac{\Delta\mathbf{K}}{\Delta x} \cdot \mathbf{u} + \frac{d\mathbf{F}_{St}}{dx} + \frac{d\mathbf{F}_{Ae}}{dx} \tag{15}$$

$$\frac{d\mathbf{F}_{Ae}}{dx} = \frac{\Delta\mathbf{F}_{Ae_0}}{\Delta x} + q \cdot \mathbf{S}^{\mathbf{T}} \cdot \mathbf{P} \cdot \mathbf{A}_{C_P} \cdot \mathbf{S} \cdot \frac{d\mathbf{u}}{dx} + q \cdot \mathbf{S}^{\mathbf{T}} \cdot \frac{\Delta\mathbf{P}}{\Delta x} \cdot \mathbf{A}_{C_P} \cdot \mathbf{S} \cdot \mathbf{u} + q \cdot \mathbf{S}^{\mathbf{T}} \cdot \mathbf{P} \cdot \frac{\Delta\mathbf{A}_{C_P}}{\Delta x} \cdot \mathbf{S} \cdot \mathbf{u} \tag{16}$$

The derivative parts that are calculated through finite differencing are marked by using Δ for the difference quotient instead of the differential quotient. Through that, no derivative data has to be exchanged across program boundaries and communication between programs can be limited to analysis evaluation calls. This reduces the complexity of data transfer in the framework. Choosing the step size for the finite differences carefully, the results of semi-analytical gradient calculation closely match the analytical gradients.

Thus, semi-analytical and numerical gradient calculation allow sensitivity analysis with respect to shape design variables in this framework by calling *DescartesNDB* once per shape design variable to receive perturbed analysis meshes. In case of the numerical gradient calculation, all analyses are performed completely for each design variable and the initial state. For semi-analytical gradients, the perturbed meshes are used to calculate the derivative parts marked in Eq.(15) and Eq.(16) with a subsequent analytical solution of the overall system of equations. In order to benefit from the computational efficiency and accuracy of the already implemented analytical gradient calculation for design variables other than shape variables (e.g. sizing), the framework allows combination of these methods depending on the design variable type.

5. Optimization of Generic UAV Wing

To examine the capabilities of the developed multidisciplinary shape optimization framework, a high aspect ratio wing of a generic unmanned aerial vehicle is studied. Its initial design has a rectangular planform with an aspect ratio of 20 and a wing span of 20 meters. This form was chosen in order to provide a neutral conceptual starting point for the shape optimization. A symmetric NACA0024 profile describes the airfoil of the wing. The CPACS parametric model of the right half of the wing is built up of 10 segments of $1\,m$ length each providing 11 sections (boundaries of the segments), at which shape design variables can be defined. The internal structural layout specified in the CPACS data set is conventional with 2 spars (at 15 % and 60 % chord) and 12 ribs (10 equally spaced span wise plus one at root and tip end). Both an *AVL* model as well as a structural FE model for *LAGRANGE* are created from the CPACS definition (Figure 4). The finite element model is built out of aluminium using 2D shell elements for skin, ribs and spars as well as 1D rods and bars for spar caps and stringers. The initial thickness for the skin is varied from root $3\,mm$ to tip $1\,mm$ and $2\,mm$ for ribs and spars (Figure 4). With these values, the mass of the modelled FE structure sums up to $193\,kg$. A maximum take off mass of $2500\,kg$ for half the aircraft including this FE structural weight is assumed. For the aerodynamic *AVL* model, the 10 segments of the CPACS definition are meshed with 10×5 equally distributed panel each, except the outermost segment, which has 10×10 panel with a span wise sine distribution (Figure 4).

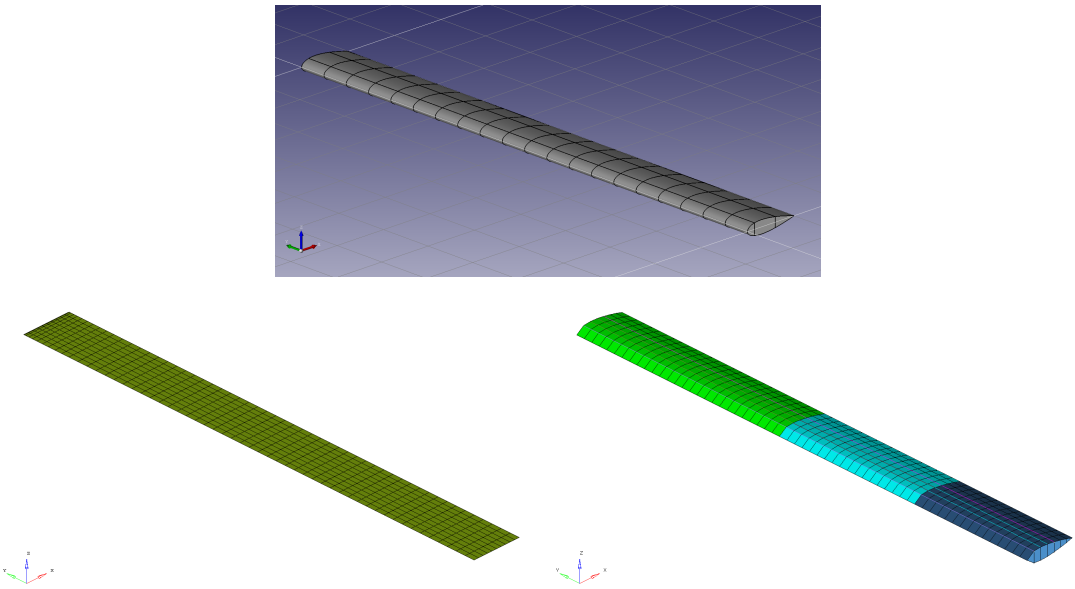

Figure 4: Models of the UAV wing in *DescartesNDB*, *LAGRANGE* and *AVL* (clockwise)

5.1 Aeroelastic Induced Drag Optimization

Two optimizations were conducted with this model. The objective of the first optimization was to minimize the induced drag during cruise conditions. For this, one load case was defined that simulates a $1g$ cruise flight at $7500\,m$ altitude with a Mach number of 0.28. In addition to the objective function of induced drag, a trimming constraint was defined to fix the aerodynamic lift force matching $2500\,kg$ at $1g$. Eleven shape design variables were defined by setting the chord length of each of the eleven CPACS sections as variable. This means that the plan form of the wing could be altered by changing the chord length between $300\,mm$ and $1500\,mm$. Also, the airfoil thickness was affected by these shape variables, since the thickness-to-chord ratio of the NACA profile was kept constant throughout the optimization. Additionally, the angle of attack was included as a design variable so that the optimizer could constantly trim the equilibrium of forces during optimization, which was enforced via the mentioned trimming constraints. With this defined criteria model, the optimization only regarded the aerodynamic attributes of the elastic wing when minimizing the induced drag, as no structural responses (e.g. stresses, strain etc.) were constrained. The resulting wing shape of this optimization run can be seen in Figure 5.
Figure 6 shows the span wise lift distribution of the elastic wing. The green line represents the initial state. It can be seen that the optimized state (red line) adapts closely to the elliptic distribution (black dashed line), which is mathematically the ideal distribution for these problems [10]. As expected, the

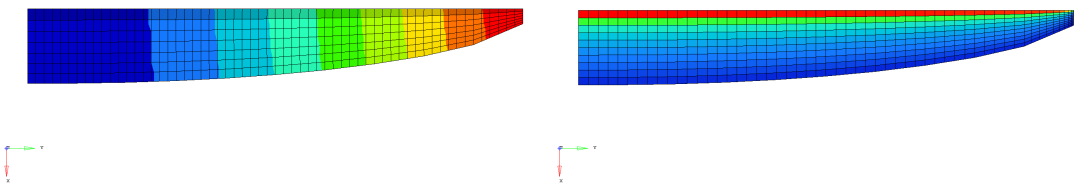

Figure 5: Optimization 1: Resulting shape of analysis models (FE with z-displacements, *AVL* with pressure distribution)

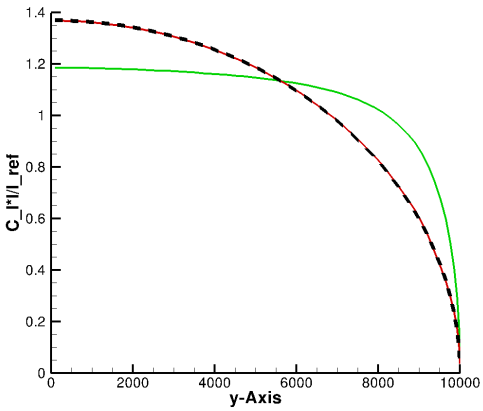

Figure 6: Optimization 1: Elastic span wise lift distribution (green: initial, red: optimized, black: aerodynamic ideal)

elliptic shape can also be seen reflected in the projected area of the analysis models (Figure 5). With this, the induced drag coefficient for the deformed wing could be reduced compared to the initial rectangular design by about 8 % at constant lift force while the mass of the wing increased by roughly 20 % through general increase in chord length.

5.2 Aeroelastic Induced Drag Optimization with Structural Criteria

The second optimization represents an extension of the first task by considering structural criteria as well. Thus, two more design driving load cases were added to the $1g$ cruise load case from before. The induced drag objective function is only defined for the $1g$ cruise case and, therefore, unaffected by the two additional load cases. A $-1g$ and a $+2.5g$ load case were defined including their respective trimming constraints and trimming variables. The shape design variable definition from the first optimization remained unchanged. To respect the structural criteria, von-Mises stress constraints were specified for all finite elements incorporating a safety factor of 1.5 summing up to 3300 constraints. Savings in structural FE mass were accounted for by the trimming constraints which were now defined using the sum of gravitational and aerodynamic forces instead of simply the target aerodynamic lift force. This means that weight savings lead to lower required aerodynamic lift. Additionally to the 11 chord length variables and the three trimming variables, 6 structural sizing design variables for the FE model skin thickness were included (see colours in Figure 4 bottom right). The upper as well as the lower skin were each divided span wise into 3 sizing variables that could vary between $0.8\,mm$ and $5\,mm$ thickness.

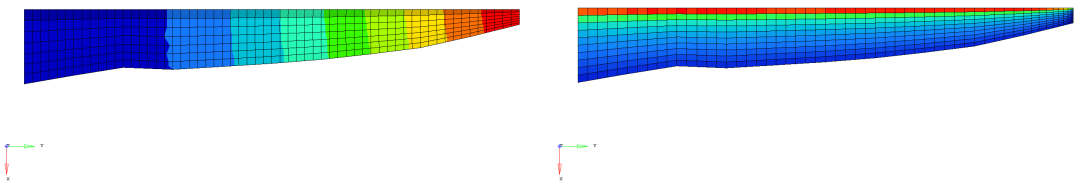

Figure 7: Optimization 2: Resulting shape of analysis models (FE with z-displacements, *AVL* with pressure distribution)

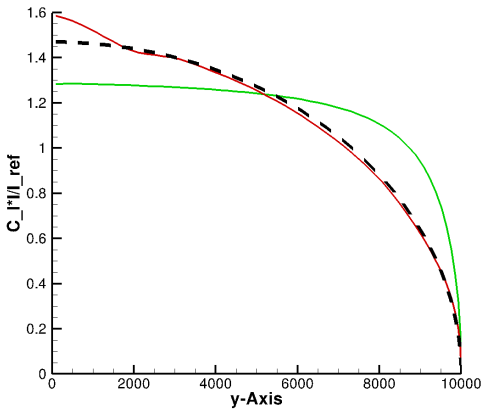

Figure 8: Optimization 2: Elastic span wise lift distribution (green: initial, red: optimized, black: aerodynamic ideal)

Figures 7 and 8 show that the second optimization did not reach the elliptic wing shape or lift distribution as the first one did. In the vicinity of the wing root the chord length was increased to the maximum gage of $1500\,mm$, which is apparent in the increased lift generation there. The reason for this measure was found to be the critical stress constraints in the skin elements in that region. These constraints

were satisfied through increasing the wing height via the constant lift-to-chord ratio while decreasing skin thickness there. Through these measures, the elastic induced drag could be decreased by around 10 % and the wing structural FE mass by 12 % with respect to the initial rectangular configuration (total lift force also decreased due to these savings). One has to mention, that the initial induced drag was higher for this optimization than the first one, caused by increased lift enforced through the modified trimming constraint definition.
A manual test was conducted to understand why the optimizer sacrificed an ideal lift distribution in order to satisfy the stress constraints instead of obtaining an ideal lift distribution while adjusting the sizing variables to meet the constraints. Hence, the resulting shape of the second optimization was modified manually to generate an ideal elliptic distribution comparable to the first result and the skin design variables were adjusted to satisfy the stress constraints. This, however, increased the structural mass necessitating a higher aerodynamic lift force through the trimming constraints. After trimming to equilibrium of forces, the elastic induced drag value lay above the one found by the second optimization due to a higher lift coefficient. Thus, the optimizer found a better overall solution by diverging from the ideal aerodynamic state. This shows how the interdependency of disciplines can cause the combined optimum to deviate from the known optima for individual disciplines.

6. Summary and Outlook

The shown example underlines the importance of concurrent consideration of design driving phenomena in order to find a design that exhibits good overall performance characteristics. Therefore, multidisciplinary design optimization combined with broad design criteria can streamline the search for globally feasible designs during the conceptual design phase. Future work for the presented framework will include implementation of higher order aerodynamic solvers as well as addition of other disciplines (e.g. radar cross section, mass etc.). Higher fidelity analysis methods (e.g. Navier-Stokes) will also be included in the framework for result verification of the optimized parametric models.

7. Acknowledgements

Parts of this development have been realized in the course the German national research project AeroStruct, funded by the Federal Ministry of Economics and Technology.

8. References

[1] E. Albano and W.P. Rodden. "A Doublet Lattice Method for Calculating Lift Distributions on Oscillating Surfaces in Subsonic Flows". In: *AIAA 6th Aerospace Sciences Meeting*. 1968.

[2] M. Drela and H. Youngren. *AVL 3.30 User Primer*. 2010.

[3] L. Fornasier. "HISSS - A Higher-Order Subsonic/Supersonic Singularity Method For Calculating Linearized Potential Flow". In: *AIAA 17th Fluid Dynamics, Plasma Dynamics, and Lasers Conference*. 1984.

[4] Sven Hedman. *Vortex Lattice Method For Calculation Of Quasi Steady State Loadings On Thin Elastic Wings In Subsonic Flow*. Tech. rep. Flygtekniska Försöksanstalten, 1966.

[5] Joseph Katz and Allen Plotkin. *Low-Speed Aerodynamics*. Ed. by Michael J. Rycroft and Wei Shyy. 2nd. Cambridge University Press, 2001.

[6] S. Kuzmina, F. Ishmuratov, and V. Kuzmin. "Minimization Of Induced Drag Of Elastic Airplane". In: *10th AIAA/ISSMO Multidisciplinary Analysis and Optimization Conference*. 2004.

[7] Carsten M. Liersch and Martin Hepperle. "A Distributed Toolbox For Multidisciplinary Preliminary Aircraft Design". In: *CEAS Aeronautical Journal* 2 (2011), pp. 57–68.

[8] Open CASCADE S.A.S. *Open CASCADE Technology - 3D modeling & numerical simulation*. `www.opencascade.org`. Apr. 2013.

[9] Gerd Schuhmacher et al. "Multidisciplinary Airframe Design Optimisation". In: *28th International Congress of the Aeronautical Sciences*. 2012.

[10] Erich Trefftz. "Prandtlsche Tragflächen- und Propeller-Theorie". In: *Zeitschrift für angewandte Mathematik und Mechanik* 1 (1921), pp. 206–218.